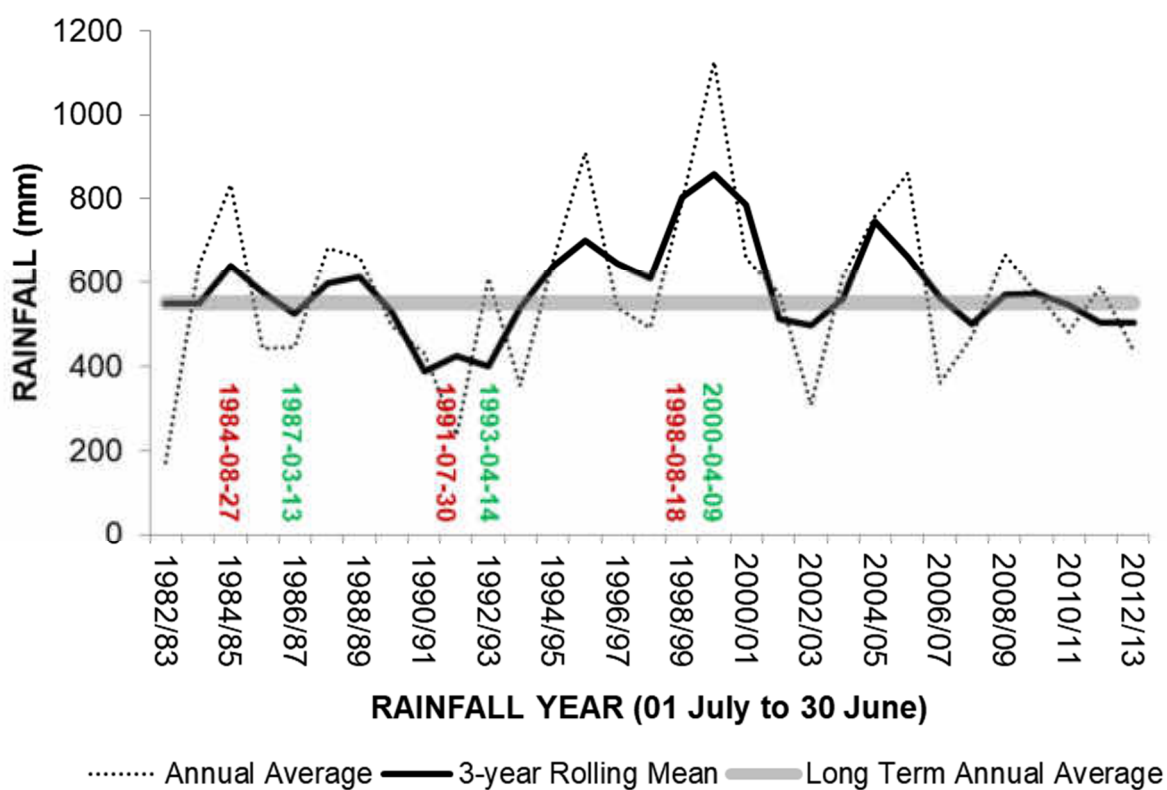
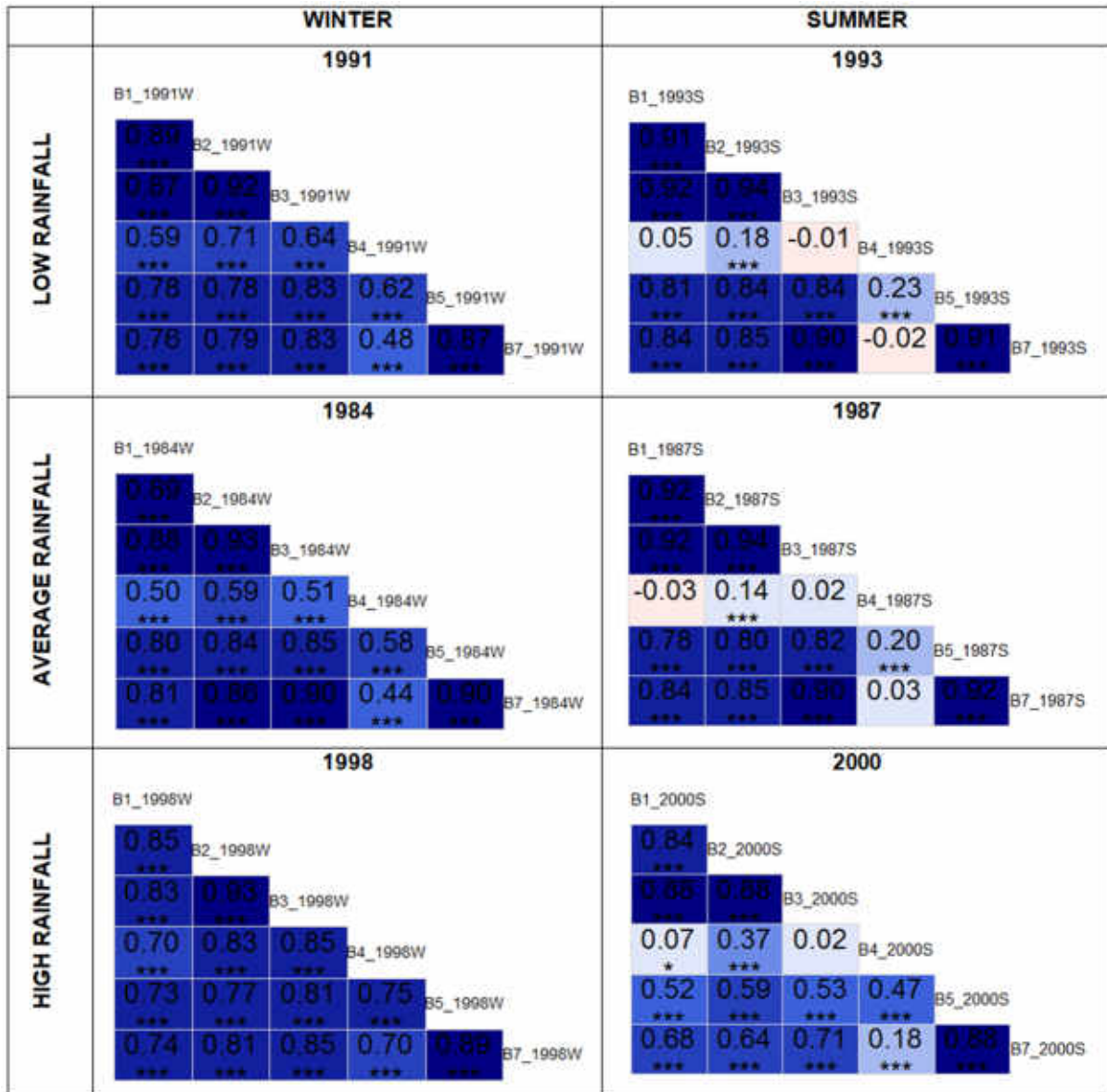


## Quantifying spatiotemporal drivers of environmental heterogeneity in Kruger National Park, South Africa



**Fig. S2.1:** Annual rainfall (dotted line) and three-year rolling mean (solid blue line) of Skukuza rainfall records from 1982 - 2013. Solid grey line indicates long-term annual mean and arrows indicates winter (red) and summer (green) Landsat scenes selected.



**Fig. S2.2:** Correlogram (graphical display of a correlation matrix) of bands values for each Landsat scene. Cells shaded blue are positively correlated, those shaded red are negatively correlated and the intensity of the shades indicate the level of the correlation value. The actual values with significance levels (\*  $p < 0.01$ ; \*\*  $p < 0.001$ ; \*\*\*  $p < 0.0001$ ) are also illustrated (Wright 2016).

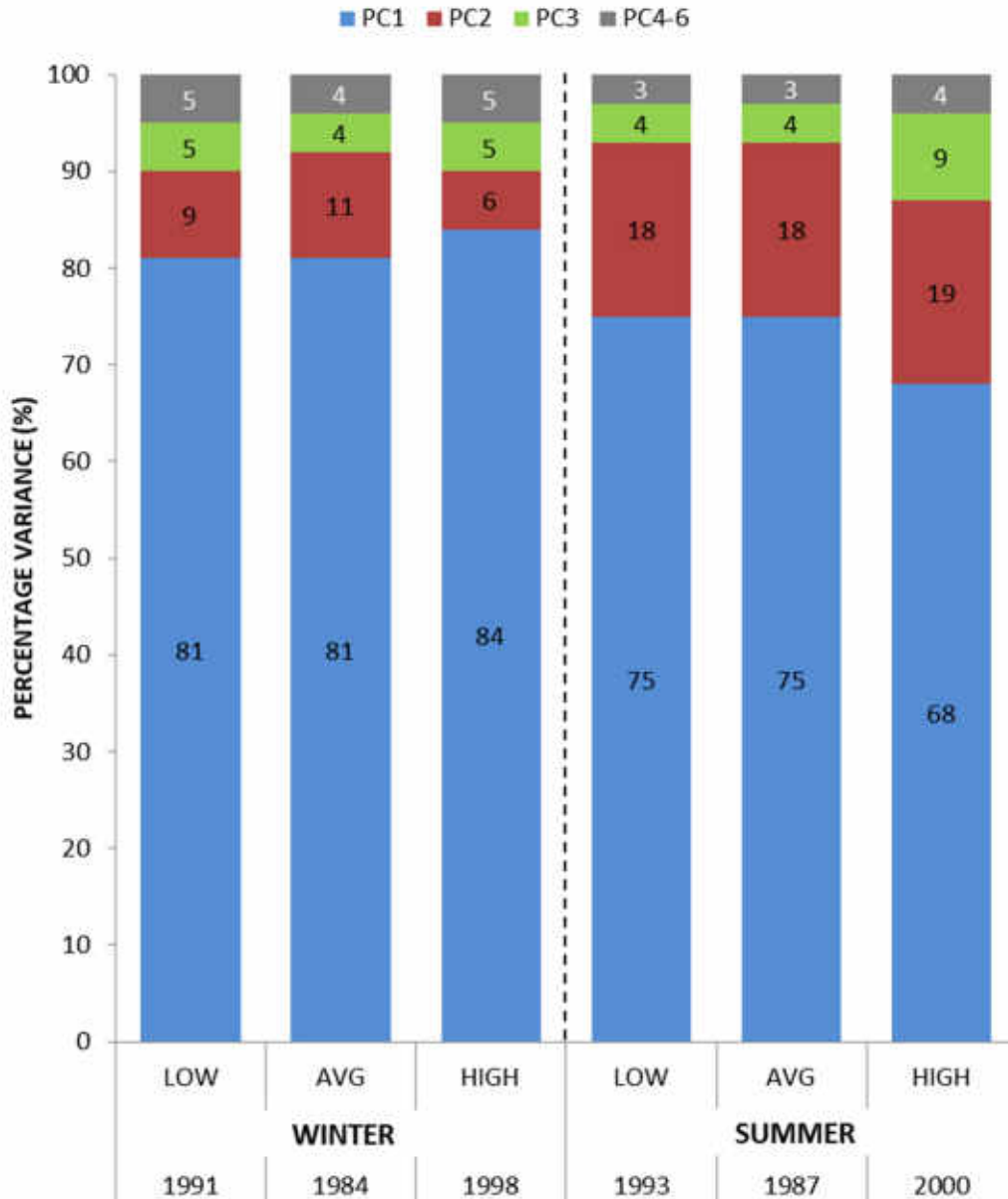


**Fig. S2.3:** Difference in the percentage variance accounted for in PC1, PC2, PC3 and PCs 4, 5 and 6 across different image dates sorted by a three-year rolling mean of rainfall (low-average-high) and season (winter-summer). In general, the proportion of variance accounted for by PC1, for example, decreases from winter to summer. In summer months, this decreases from low to high rainfall. While patterns are less clear within winter months and average rainfall conditions, possibly because of the relatively large variation in rainfall between individual years.

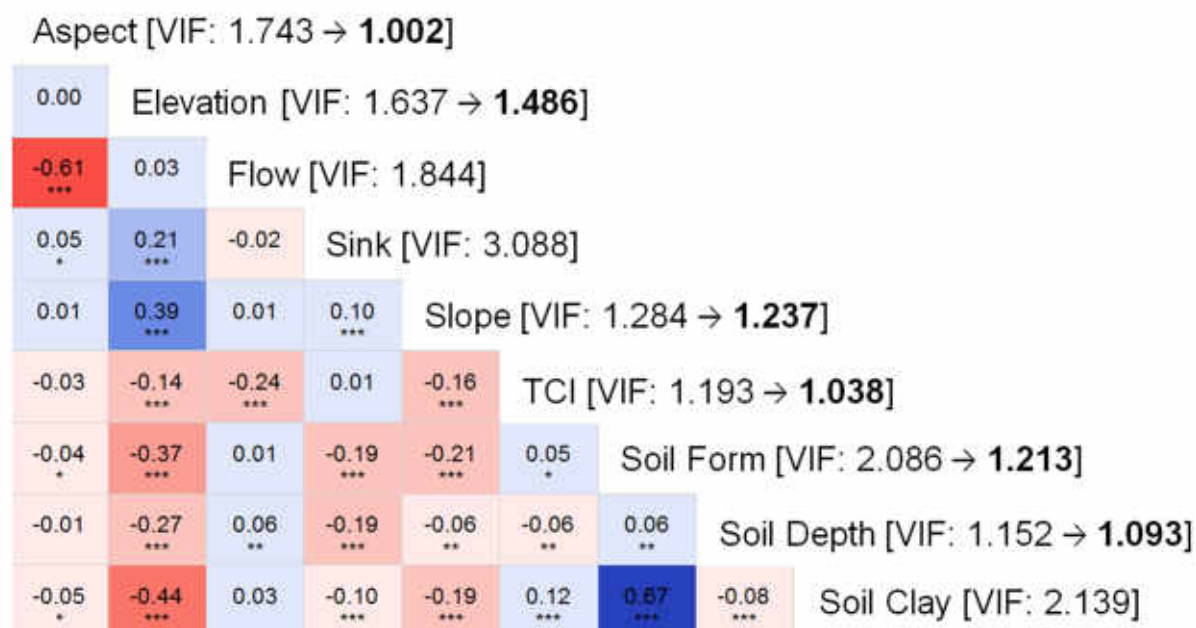


**Fig. S2.4:** Correlogram (graphical display of a correlation matrix) of physical landscape covariates (Wright 2016). Cells shaded blue are positively correlated, those shaded red are negatively correlated and the intensity of the shades indicate the level of the correlation value. The actual values with significance levels (\*  $p < 0.01$ ; \*\*  $p < 0.001$ ; \*\*\*  $p < 0.0001$ ) are also illustrated. Variance Inflation Factors (VIF) are calculated for these physical landscape covariates by excluding highly correlated variables and repeating VIF calculations until all values were below 1.5 (Naimi 2015). Flow and aspect are significantly negatively correlated (-0.63) while soil form and soil clay content are significantly positively correlated (0.67). Flow and soil clay as well as watershed area (sink) have higher VIF values and are therefore removed from further analyses.

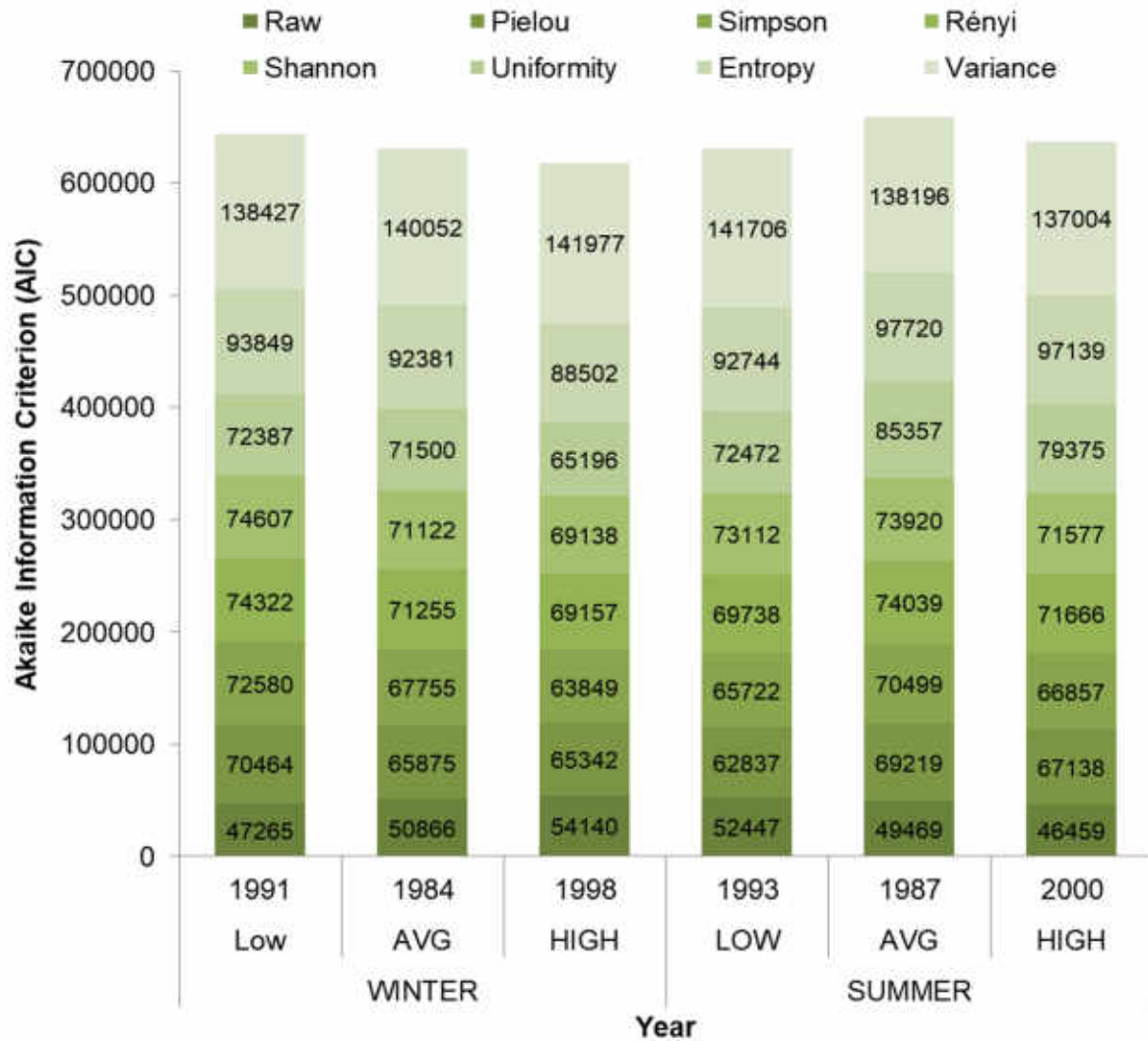


**Fig. S2.5:** Difference in AIC scores for local GWR models of raw PC values, different diversity indices (Shannon, simpson, renyi, pielou) and textural variance measures (uniformity, entropy and variance) of the spectral response and physical landscape properties by season and rainfall condition. Unilaterally, models with raw PC values representing spectral variation were better able to balance model fit and complexity, as indicated by the notably lower AIC scores.



**Table S2.3:** Geographically Weighted Regression results illustrating local differences between relationships of physical landscape elements with Landsat spectral variation across different years. The first (1stQu), second (Median) and third (3rdQu) order quartiles show the local variability of resulting coefficient estimates. The inter-quartile range (IQR) summarise the range where 50% of all coefficient estimate values fall. Leung et al.'s (2000) F statistic (F3) tests the spatial non-stationarity of each in dependent variable's coefficient using numerator degrees of freedom (nDF) and denominator degrees of freedom (dDF).

		1stQu	Median	3rdQu	IQR	F3	nDF	dDF	P	
1991	X.Intercept.	865.30	875.60	880.20	14.90	6.87	550	2380	< 0.0001	***
	aspect	-3.99	-1.21	-0.72	-3.27	0.98	1449	2380	0.6962	
	dem	-12.92	-1.88	1.24	-11.68	4.57	1254	2380	< 0.0001	***
	slope	-4.73	-1.40	-0.45	-4.28	1.26	360	2380	0.0013	**
	tci	-6.64	-3.26	-1.99	-4.66	2.99	344	2380	< 0.0001	***
	soil.form	-5.58	-0.80	0.42	-5.16	1.36	206	2380	0.0007	***
	soil.depth	-3.44	-0.64	0.30	-3.13	1.34	41	2380	0.0730	.
	<b>Number nearest neighbours: 199</b>						<b>Adjusted R<sup>2</sup>: 0.392</b>			
<b>Quasi-global R<sup>2</sup>: 0.456</b>						<b>AICc: 18944.54</b>				
1984	X.Intercept.	863.40	908.40	918.80	55.40	7.89	485	2329	< 0.0001	***
	aspect	-0.06	-0.01	-0.01	-0.06	1.00	1432	2329	0.5250	
	dem	-0.44	-0.06	0.04	-0.40	3.92	1236	2329	< 0.0001	***
	slope	-0.43	-0.06	0.02	-0.40	1.11	368	2329	0.0843	.
	tci	-0.26	-0.09	-0.04	-0.22	2.85	363	2329	< 0.0001	***
	soil.form	-0.19	-0.04	0.00	-0.19	2.53	138	2329	< 0.0001	***
	soil.depth	-0.14	-0.04	-0.01	-0.13	2.10	30	2329	0.0004	***
	<b>Number nearest neighbours: 157</b>						<b>Adjusted R<sup>2</sup>: 0.439</b>			
<b>Quasi-global R<sup>2</sup>: 0.494</b>						<b>AICc: 20560.98</b>				
1998	X.Intercept.	655.50	723.20	737.60	82.10	7.72	475	2316	< 0.0001	***
	aspect	-0.13	-0.03	-0.02	-0.11	1.75	1427	2316	< 0.0001	***
	dem	-0.89	-0.32	-0.12	-0.77	5.82	1230	2316	< 0.0001	***
	slope	-0.67	-0.17	-0.07	-0.60	1.15	371	2316	0.0319	*
	tci	-0.31	-0.14	-0.08	-0.23	2.19	368	2316	< 0.0001	***
	soil.form	-0.23	-0.04	0.00	-0.23	1.71	127	2316	< 0.0001	***
	soil.depth	-0.17	-0.04	-0.01	-0.16	1.47	31	2316	0.0479	*
	<b>Number nearest neighbours: 149</b>						<b>Adjusted R<sup>2</sup>: 0.315</b>			
<b>Quasi-global R<sup>2</sup>: 0.409</b>						<b>AICc: 21810.65</b>				
1993	X.Intercept.	601.40	656.50	671.00	69.60	11.67	475	2316	< 0.0001	***



	aspect	-0.06	-0.02	-0.01	-0.05	1.25	1427	2316	< 0.0001	***
	dem	-0.97	-0.39	-0.23	-0.74	4.74	1230	2316	< 0.0001	***
	slope	-1.23	-0.16	-0.05	-1.18	1.50	371	2316	< 0.0001	***
	tci	-0.30	-0.06	-0.03	-0.27	1.60	368	2316	< 0.0001	***
	soil.form	-0.28	-0.03	0.01	-0.26	1.84	127	2316	< 0.0001	***
	soil.depth	-0.23	-0.04	-0.01	-0.22	1.27	31	2316	0.1467	
	<b>Number nearest neighbours: 149</b>					<b>Adjusted R<sup>2</sup>: 0.565</b>				
	<b>Quasi-global R<sup>2</sup>: 0.635</b>					<b>AICc: 21298.95</b>				
1987	X.Intercept.	802.80	917.90	940.10	137.30	13.58	475	2316	< 0.0001	***
	aspect	-0.07	-0.01	0.00	-0.07	1.32	1427	2316	< 0.0001	***
	dem	-1.30	-0.28	-0.05	-1.25	10.88	1230	2316	< 0.0001	***
	slope	-1.13	-0.14	-0.04	-1.09	2.02	371	2316	< 0.0001	***
	tci	-0.31	-0.07	-0.03	-0.29	2.58	368	2316	< 0.0001	***
	soil.form	-0.35	-0.02	0.03	-0.33	2.37	127	2316	< 0.0001	***
	soil.depth	-0.34	-0.04	0.00	-0.34	2.01	31	2316	0.0008	***
		<b>Number nearest neighbours: 149</b>					<b>Adjusted R<sup>2</sup>: 0.567</b>			
	<b>Quasi-global R<sup>2</sup>: 0.720</b>					<b>AICc: 19696.98</b>				
2000	X.Intercept.	439.60	450.70	457.40	17.80	4.74	529	2363	< 0.0001	***
	aspect	-0.03	-0.01	0.00	-0.03	1.58	1444	2363	< 0.0001	***
	dem	-0.24	-0.05	0.01	-0.23	3.44	1250	2363	< 0.0001	***
	slope	-0.23	-0.03	0.02	-0.20	1.20	363	2363	0.0105	*
	tci	-0.01	0.02	0.05	0.04	3.77	349	2363	< 0.0001	***
	soil.form	-0.02	0.01	0.02	0.00	1.32	185	2363	0.0032	**
	soil.depth	-0.10	-0.02	-0.01	-0.09	2.54	35	2363	< 0.0001	***
		<b>Number nearest neighbours: 183</b>					<b>Adjusted R<sup>2</sup>: 0.255</b>			
	<b>Quasi-global R<sup>2</sup>: 0.234</b>					<b>AICc: 19061.62</b>				

*Model settings: gwr.basic (Kernel function = bisquare; adaptive bandwidth = no of nearest neighbours; regression points = same locations as observations; distance metric = Euclidean distance metric) (Gollini et al. 2015)*



**Table S2.4:** Comparatively, only 57% and 62% of the variability in plant species richness was captured by raw surface reflectance PC values and raw physical landscape properties respectively. The first (1stQu), second (Median) and third (3rdQu) order quartiles show the local variability of resulting coefficient estimates. The inter-quartile range (IQR) summarise the range where 50% of all coefficient estimate values fall. Leung et al.'s (2000) F statistic (F3) tests the spatial non-stationarity of each in dependent variable's coefficient using numerator degrees of freedom (nDF) and denominator degrees of freedom (dDF).

	Q1	Med	Q3	IQR	F3	nDF	dDF	P	
Intercept	-	34.69	122.9	-	2.8	231.0	566.5	<	**
	2504.00		0	2381.10	9	7	4	0.0001	*
PC 1991	-0.38	0.04	0.19	-0.19	1.4	213.6	566.5	<	**
					4.2	264.8	566.5	<	**
PC 1993	-1.82	-0.07	0.02	-1.80	0	6	4	0.0001	*
					3.3	218.9	566.5	<	**
PC 1984	-0.71	-0.01	0.07	-0.65	0	3	4	0.0001	*
					1.7	250.7	566.5	<	**
PC 1987	-1.03	0.04	0.13	-0.90	2	5	4	0.0001	*
					1.4	217.5	566.5	<	**
PC 1998	-0.82	-0.01	0.08	-0.74	2	0	4	0.0008	*
					3.0	201.0	566.5	<	**
PC 2000	-0.73	0.05	0.15	-0.58	0	0	4	0.0001	*
Number of nearest neighbours: 76									
Adjusted R <sup>2</sup> : 0.566									
AICc:									
5766.01									
Intercept	71.14	127.0	448.6	377.46	5.3	226.4	553.4	<	**
		0	0		9	4	6	0.0001	*
aspect	0.00	0.01	0.06	0.06	1.1	341.2	553.4	<	**
					8	5	6	0.0443	*
dem	-0.06	0.02	0.41	0.35	6.0	354.7	553.4	<	**
					2	8	6	0.0001	*
sink	0.00	0.00	0.03	0.02	8.3	223.1	553.4	<	**
					6	1	6	0.0001	*
slope	-0.82	0.79	9.89	9.06	7.6	161.9	553.4	<	**
					0	1	6	0.0001	*
tc1	-0.48	0.13	7.15	6.67	1.7	132.8	553.4	<	**
					1	8	6	0.0001	*
soil.form	-0.05	0.94	5.23	5.18	0.7	103.1	553.4		
					8	5	6	0.9411	
soil.depth	-0.32	0.78	8.43	8.12	0.9		553.4		
					4	98.69	6	0.6340	
Number of nearest neighbours: 85									
Adjusted R <sup>2</sup> : 0.621									
AICc: 5694.72									

*Model settings: gwr.basic (Kernel function = bisquare; adaptive bandwidth = no of nearest neighbours; regression points = same locations as observations; distance metric = Euclidean distance metric) (Gollini et al. 2015).*

## Long-term rainfall regression surfaces for the Kruger National Park, South Africa: A spatiotemporal review of patterns from 1981-2015

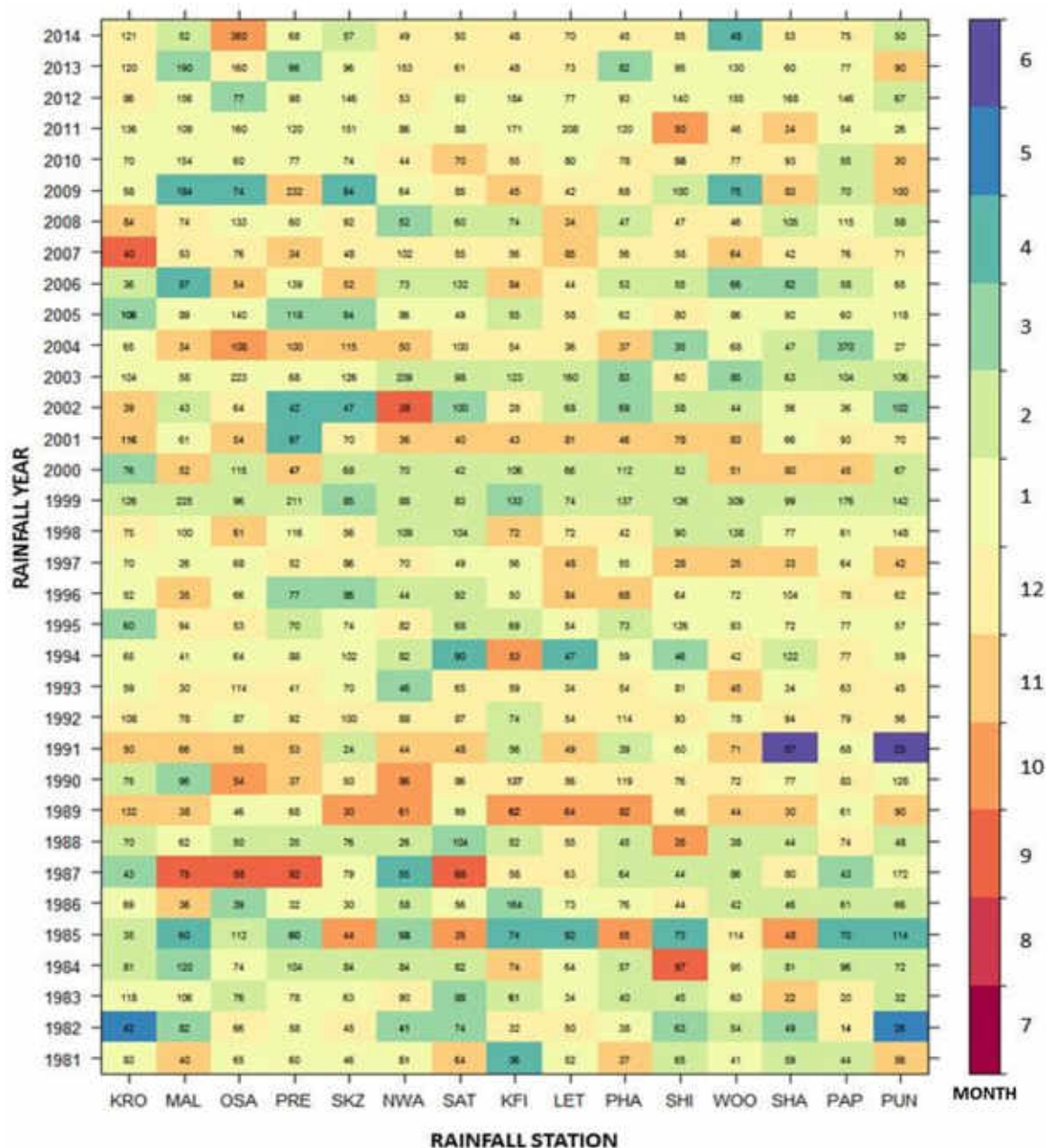


**Fig. S3.1:** Level plot of month in which the maximum daily rainfall was received for a particular rainfall year and selected stations in Kruger from 1981-2015. The maximum value is displayed in each year-month-station cell.

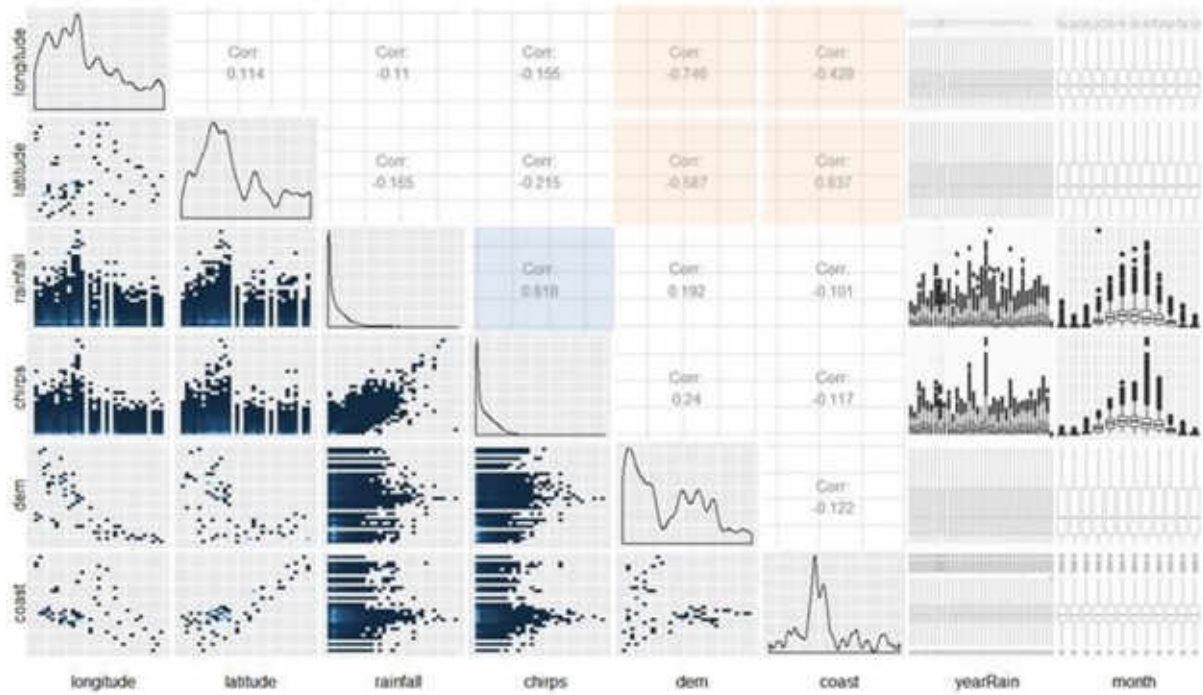


**Fig. S3.2:** Visualisation of correlation matrix confirming no problems of collinearity between variables but highlighting inherent spatial autocorrelation between spatial covariates.

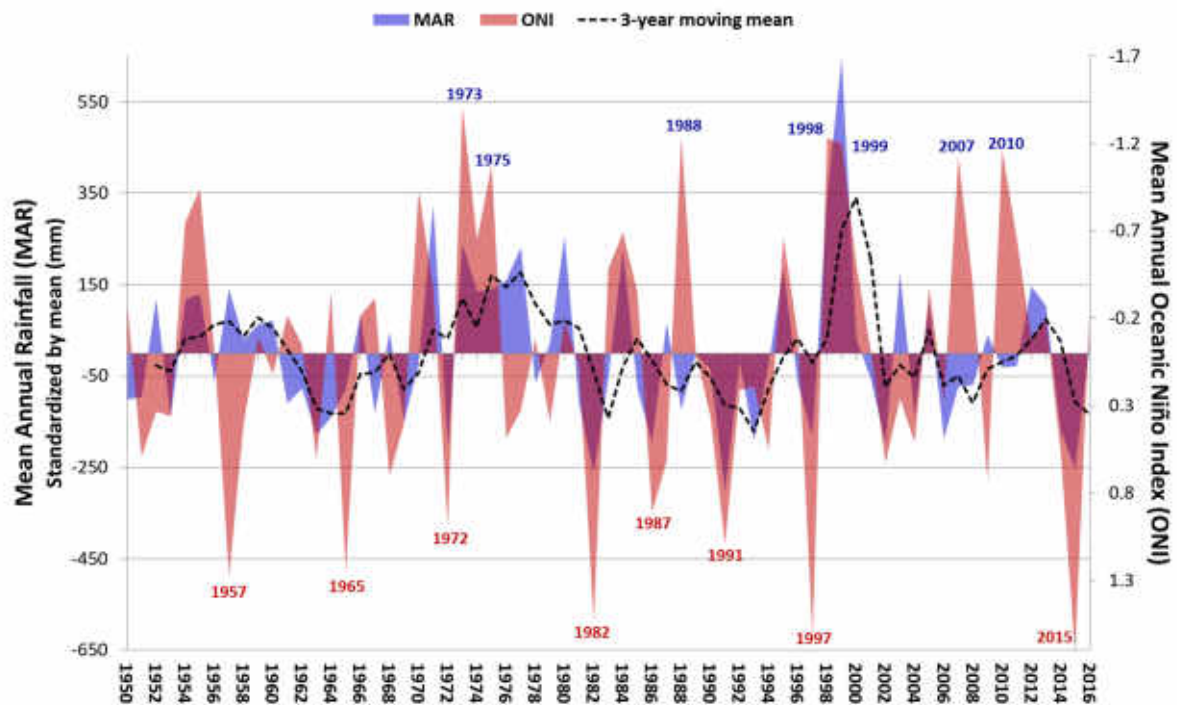


**Fig. S3.3:** The Mean Annual Rainfall (MAR) of the Kruger National Park and the Oceanic Niño Index (ONI) identifying El Niño (warm) and La Niña (cool) events in the tropical Pacific from 1950-2015. Years labelled red represent strong to very strong El Niño events, which typically decrease rainfall across Southern Africa. Years labelled blue indicate strong La Niña events, where rainfall is generally increased (Huang et al., 2017; data accessed 19 October 2017 from [http://origin.cpc.ncep.noaa.gov/products/analysis\\_monitoring/ensostuff/ONI\\_v5.php](http://origin.cpc.ncep.noaa.gov/products/analysis_monitoring/ensostuff/ONI_v5.php)).

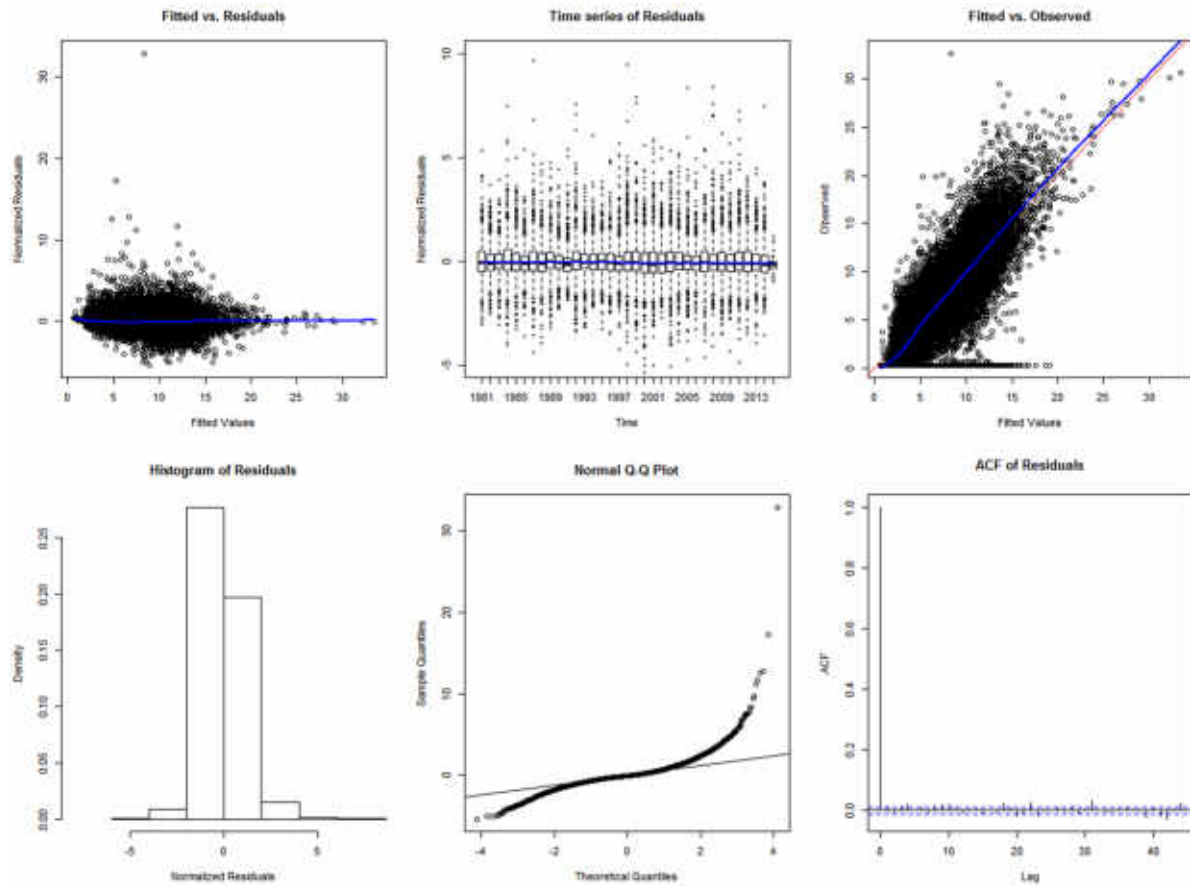


**Fig. S3.4:** Model diagnostics for GAMM (*Table S3.2 in Appendix S3*; See [1] for full GAMM equation) showing no residual temporal autocorrelation.



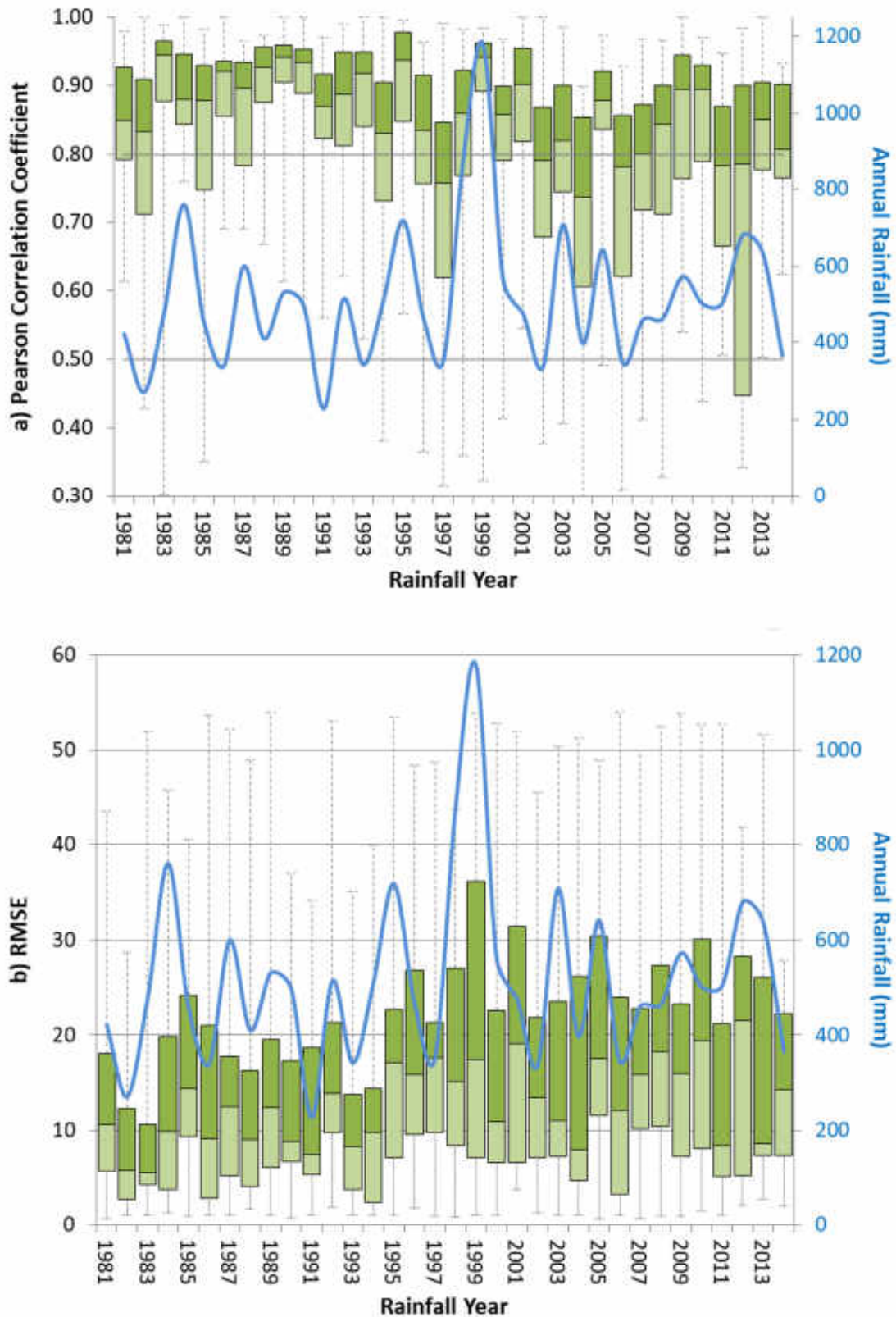


**Fig. S3.5:** Cross-validation of gridded results with monthly rainfall data from 59 stations ( $n=7645$ ) confirmed our spatiotemporal regression surfaces produced accurate predictions of monthly rainfall ( $R^2 = 0.78$ ,  $t = 107.5$ ,  $df = 7643$ ,  $p\text{-value} < 0.001$ ) with an RMSE error of 19.99 mm per year.

**Table S3.1:** Examples of some global climatological datasets that have become available in recent years (Muñoz et al. 2011; Kearney et al. 2014). (see NCAR 2014 and Sun et al. 2016 for a full summary).

Name	Description	Resolution		Reference
		Temporal	Spatial	
CHIRPS	Climate Hazards Infrared Precipitation with Stations products incorporates satellite imagery with ground station data to create gridded rainfall time series	6 hourly, daily, monthly, yearly since 1981 to present	±5km <sup>2</sup>	Funk et al. 2015
CMORPH	CPC MORPHing technique to produce global precipitation analyses from low orbiter satellites	Every 30 minutes since December 2002 to present	±8km <sup>2</sup>	Joyce et al. 2004
E-OBS	ENSEMBLES Daily gridded observational datasets	Daily from 1950 to 2016	±28km <sup>2</sup>	van der Linden and Mitchell 2009
GHCN	Global Historical Climatology Network provide numerous regional and local climate data products	Monthly from 1870 to 2014	±56km <sup>2</sup>	Menne et al. 2012
GSMaP	Global Satellite Mapping of Precipitation	Hourly from 1998 to present	±11km <sup>2</sup>	Kubota et al. 2007
PERSIANN	Precipitation Estimation from Remotely Sensed Information using Artificial Neural Networks	1 hourly, 3 hourly, 6 hourly, daily, monthly, yearly since March 2000 to present	±28km <sup>2</sup>	Sorooshian et al. 2000
TRMM	Tropical Rainfall Measuring Mission	3 hourly from 1997 to 2015	±28km <sup>2</sup>	Huffman et al. 2007
WorldClim	Set of global climate layers interpolated from observed data from 1960 to 1990	Long-term monthly average	±1km <sup>2</sup>	Hijmans et al. 2005

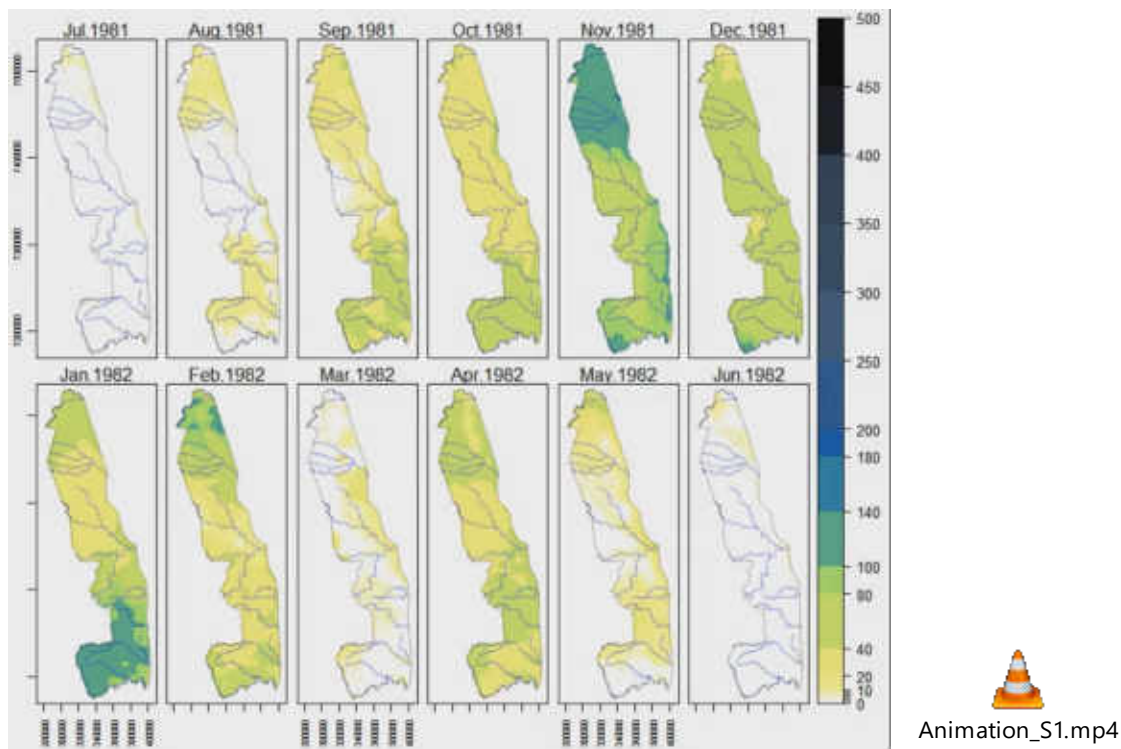


**Table S3.2:** GAMM results describing the response of ground measured rainfall as explained by its non-linear relationship with CHIRPS, elevation (DEM) and distance to the Indian Ocean coastline (DIOC) smoothed over space, seasonal cycle (within year) and long-term trend (between years).

<b>Parametric coefficients</b>	<b>Estimate</b>	<b>SE</b>	<b>t-value</b>	<b>p-value</b>
(Intercept)	6.244	0.068	92.03	< 0.001
<b>Smooth terms</b>	<b>edf</b>	<b>Ref. df</b>	<b>F-value</b>	<b>p-value</b>
s(chirps)	8.408	8.408	213.798	< 0.001
s(dem)	8.865	8.865	73.689	< 0.001
s(coast)	8.201	8.201	19.922	< 0.001
s(yearRain)	6.92	6.92	5.981	< 0.001
s(mnthRain)	4.761	10	6.711	< 0.001
ti(yearRain,mnthRain)	29.773	330	0.139	0.001
ti(chirps,dem)	7.122	7.122	6.445	< 0.001
ti(chirps,coast)	4.024	4.024	3.825	0.005
ti(chirps,yearRain)	58.225	276	0.692	< 0.001
ti(chirps,mnthRain)	8.081	76	0.177	0.025
<b>Adjusted R<sup>2</sup>: 0.73</b>	<b>Scale est: 6.504</b>	<b>n: 25296</b>		

**Table S3.3:** GAMM results describing the seasonal (within-year) and longer term (between years) trends in predicted rainfall surface layers, allowing the within year seasonal effect (mnthRain) to vary smoothly with a between year trend effect (yearRain) over space (x,y).

<b>Parametric coefficients</b>	<b>Estimate</b>	<b>SE</b>	<b>t-value</b>	<b>p-value</b>
(Intercept)	5.894	0.002	3310	< 0.0001
<b>Smooth terms</b>	<b>edf</b>	<b>Ref. df</b>	<b>F-value</b>	<b>p-value</b>
s(x,y)	28.926	29	2080.07	< 0.0001
s(yearRain)	8.998	9	8664.57	< 0.0001
s(mnthRain)	9.997	10	75107.94	< 0.0001
ti(mnthRain,yearRain)	89.963	90	2586.89	< 0.0001
ti(x,y,mnthRain)	63.821	64	524.35	< 0.0001
ti(x,y,yearRain)	63.011	64	62.53	< 0.0001
<b>Adjusted R<sup>2</sup>: 0.74</b>	<b>Scale est: 12.489</b>	<b>n: 989400</b>		



**Animation S3.1:** Animation of predicted rainfall surfaces, using the results of GAMM and the full 1km<sup>2</sup> spatiotemporal grid of associated covariates, illustrating the seasonal and annual spatiotemporal rainfall dynamics in Kruger from 1981-2015.

## Space is not 'irrelephant': Spatiotemporal distribution dynamics of elephants in response to density, rainfall, rivers and fire in Kruger National Park, South Africa

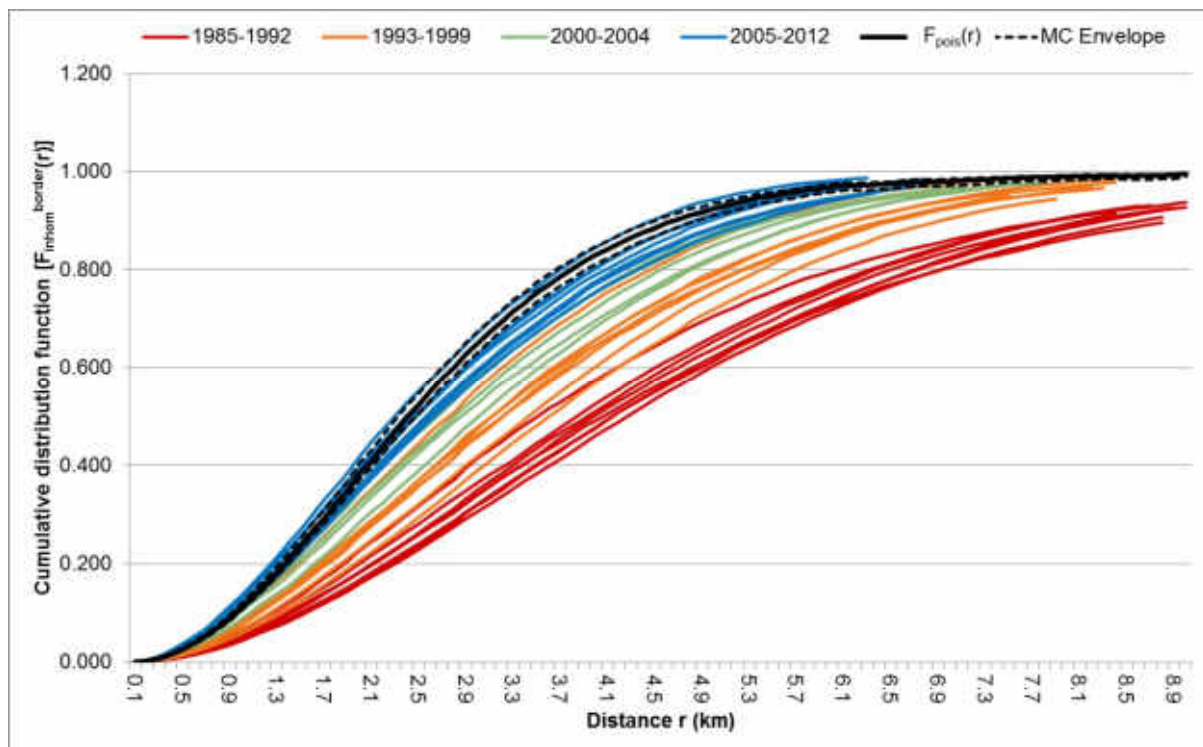


**Fig. S4.1:** Inhomogeneous empty-space function ( $F_{inhom}(r)$ ), showing the cumulative border corrected spherical contact distances (y-axis) between elephants from 1985-2012. The dashed black line indicates the average theoretical  $F_{inhom}(r)$  for all years, expected under the assumption of Complete Spatial Randomness. While the dotted black lines represent the minimum and maximum, from 1985 to 2012, of the upper and lower bounds of pointwise simulation envelopes ( $n=500$ ) for the theoretical curve  $F_{inhom}(r)$ . Elephants are significantly clustered in earlier years (e.g. 1985-2004), as  $F_{inhom}(r)$  lies well below the theoretical curve, whereas more recent years (e.g. 2010-2012) show no significant signs of clustering. The observed empty-space distances have shortened from 1985 to 2012, indicating that there is less empty-space between elephants in 2012 compared to 1985.

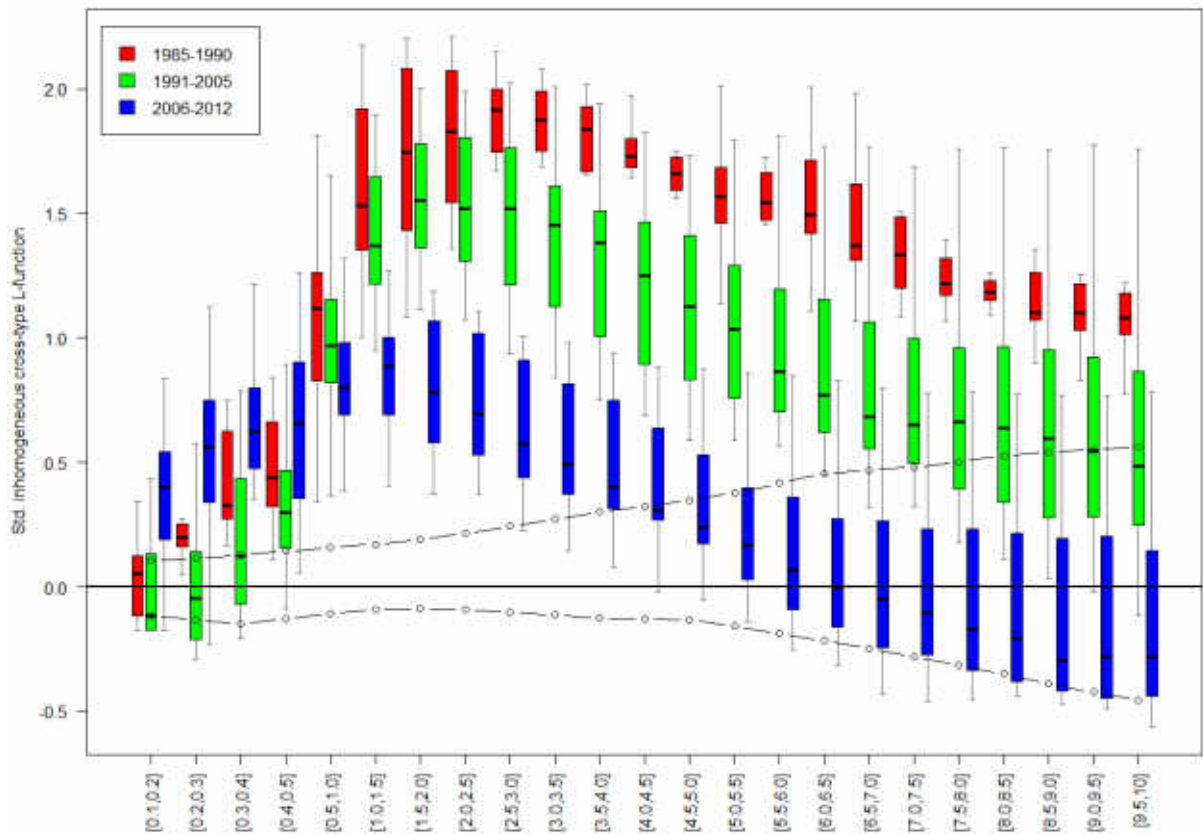


**Fig. S4.2:** The degree to which lone bull groups and mixed herds are spatially segregated (y-axis) at particular distances (x-axis) for different time periods (colour shading). Positive y-axis values indicate that bull and herd groups attract each other. Negative y-axis values indicate bull and herd groups inhibit each other. Black dotted lines represent minimum and maximum values of the standardised lower and upper bounds of pointwise simulation envelopes ( $n=500$ ) of the inhomogeneous cross-type L function for bull and herd elephant groups from 1985 to 2012. Results were standardised by subtracting the theoretical curve of random labelling from the observed, border corrected results. Values above or below the zero line indicate a positive or negative deviation from random. A small negative deviation is visible in earlier years at distances  $<1\text{km}$ , suggesting a clearer pattern of group-type segregation in these years. From distances  $>1\text{km}$ , bull and herd groups tend to cluster. This pattern however, appears to be changing as bull and mixed herd groups are forced into closer proximity as numbers increase and available empty space decreases from 1985-2012.

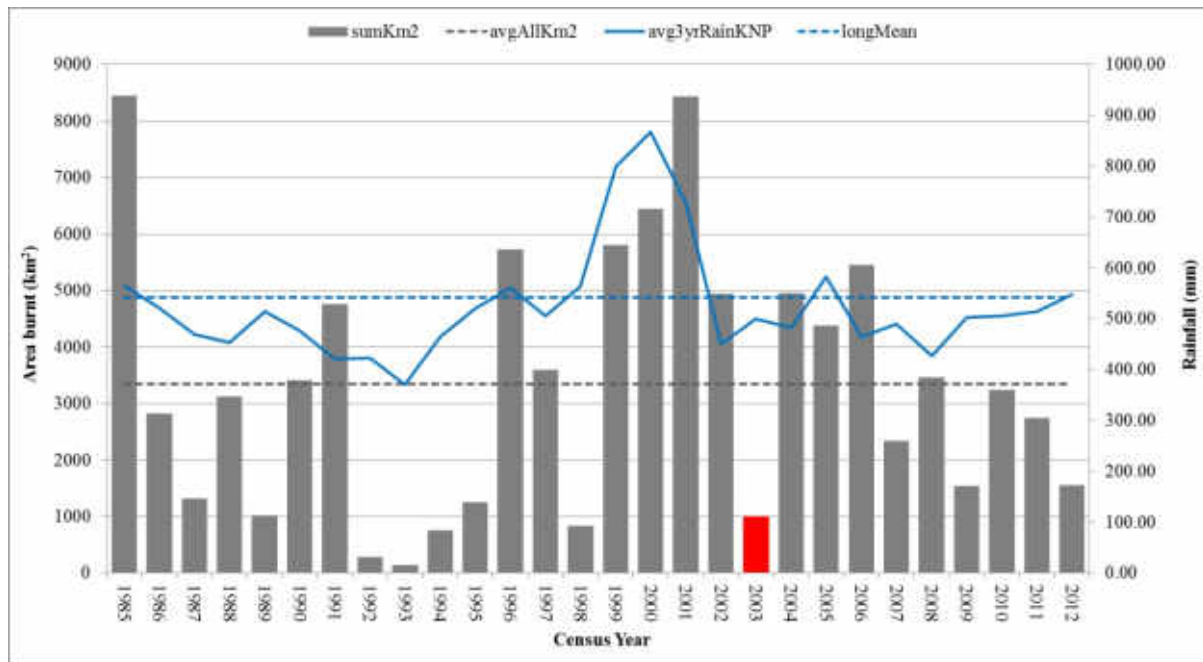


**Fig. S4.3:** Area burnt and average three-year moving rainfall average for Kruger from 1985 to 2012. Grey bars represent the total area burnt, along with the long-term mean as a dashed grey line. The blue solid line represents the three-year moving average of rainfall, along with the long-term mean as a dashed blue line. The single red bar indicates the year in which the strongest change in elephant densities occurred (see Fig. 3).

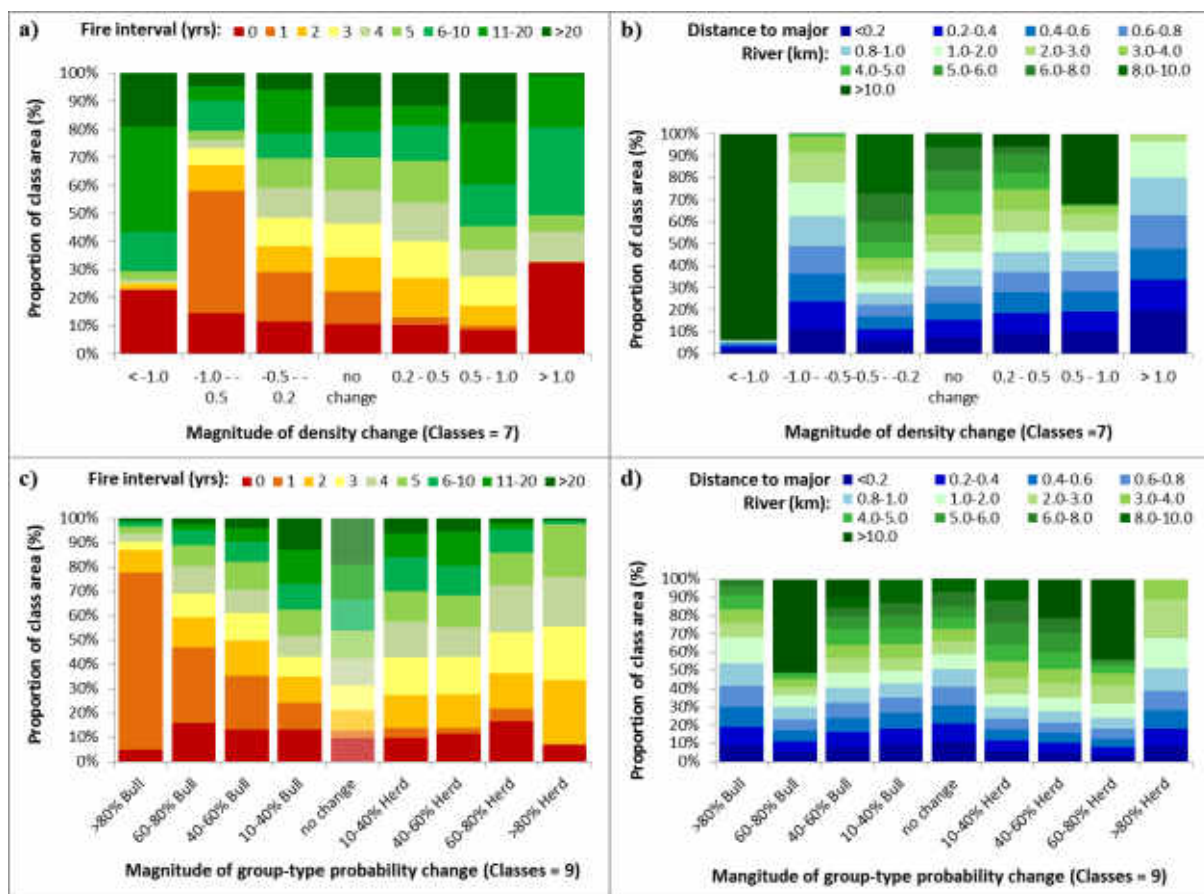
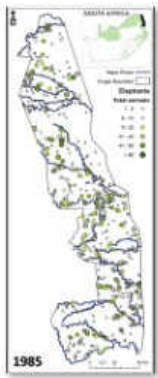


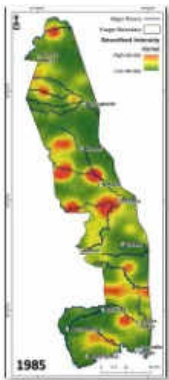
**Fig. S4.4:** Percentage of areas, under different fire frequency regimes and distances to major rivers, undergoing significant changes to overall elephant density and changes to the probabilities of encountering either elephant bull or herd groups. Panel a) illustrates the proportional areal differences of varying fire return periods in areas of significant overall elephant density change in 1998-2012 compared to 1985-1997 (BFAST,  $P < 0.05$ ). The effect of fire return period on areas of extreme density decrease ( $< 1.0$  elephant per  $\text{km}^2$ ) or increase ( $> 1.0$  elephant per  $\text{km}^2$ ) is unclear. However in general, areas undergoing significant decreases in elephant density have experienced more frequent fires (darker reds) and those areas with increasing densities less frequent fires (greens),  $\chi^2(48, 63) = 156.66$ ,  $p < 0.0001$ ). Panel b) illustrates the proportional areal differences of varying distances to major rivers for areas of significant overall elephant density change in 1998-2012 compared to 1985-1997 (BFAST,  $P < 0.05$ ). Areas closer to major rivers (blues) are clearly dominated by significant increases to elephant densities while decreases appear to be occurring further away from these river (greens),  $\chi^2(60, 77) = 74.844$ ,  $p = 0.0939$ ). Panel c) illustrates the proportional areal differences of varying fire return periods in areas of significant group-type probability change in 1998-2012 compared to 1985-1997 (BFAST,  $P < 0.05$ ). Areas experiencing an increase in bull occurrence tend to be made up of shorter fire return intervals (more frequent fires; darker reds) while an increase in herd group occurrence is dominated by more intermediate fire frequencies (lighter greens),  $\chi^2(64, 81) = 302.39$ ,  $p < 0.0001$ ). Panel d) illustrates the proportional areal differences of varying distances for major rivers for areas of significant group-type probability change in 1998-2012 compared to 1985-1997 (BFAST,  $P < 0.05$ ). Only subtle differences are discernible for the different magnitudes of change but these are not significant,  $\chi^2(80, 99) = 72.356$ ,  $p = 0.7162$ ).





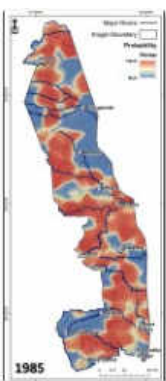
3AnimationS1.mov

**Animation S4.1:** Animation of Kruger's elephant point pattern data 1985-2012 (double-click on Fig. to start animation).



3AnimationS2.mov

**Animation S4.2:** Animated results of separate kernel smoothed intensity functions from each point pattern ( $n=28$ ) showing elephant density variation spatially, with a general increasing trend over time (double-click on Fig. to start animation).



3AnimationS3.mov

**Animation S4.3:** Animated results showing annual differences in the spatial distribution of lone bulls (shades of blue) and mixed herd groups (shades of reds). This was derived from a nonparametric analysis of spatially-varying relative risk using the `relrisk.ppp` {`spatstat`} function with kernel smoothing and edge correction (double-click on Fig. to start animation).



**Table S4.1:** Description of functions and associated R packages. The ID cross-references to the function indicated in the text. The name function is italicised as it indicates the correct wording used in the text.

ID	Function	Parameters	Name	Description	R Package	Reference
1	<i>jitter</i>			Add a small amount of noise to a numeric vector.	<i>base</i>	R Core Team (2016) R: A language and environment for statistical computing. R Foundation for Statistical Computing, Vienna, Austria. URL <a href="https://www.R-project.org/">https://www.R-project.org/</a>
2	<i>ppp</i>		Create a Point Pattern	Creates an object of class "ppp" representing a point pattern dataset in the two-dimensional plane.		
3	<i>hyperframe</i>		Hyper Data Frame	Create a hyperframe: a two-dimensional array in which each column consists of values of the same atomic type (like the columns of a data frame) or objects of the same class.		
4	<i>rescale</i>		Convert Point Pattern to Another Unit of Length	Converts a point pattern dataset to another unit of length.		
5	<i>studpermu.test</i>		Studentised Permutation Test	Perform a studentised permutation test for a difference between groups of point patterns.		
6	<i>Kinhom</i>		Inhomogeneous K-function	Estimates the inhomogeneous K function of a non-stationary point pattern.		
7	<i>Finhom</i>		Inhomogeneous Empty Space Function	Estimates the inhomogeneous empty space function of a non-stationary point pattern.		
8	<i>segregation.test</i>		Test of Spatial Segregation of Types	Performs a Monte Carlo test of spatial segregation of the types in a multitype point pattern.	<i>spatstat</i>	Baddeley A, Rubak E and Turner R (2015). Spatial Point Patterns: Methodology and Applications with R. London: Chapman and Hall/CRC Press.
9	<i>Lcross.inhom</i>	border correction, random labelling simulation expression	Inhomogeneous Cross Type L Function	For a multitype point pattern, estimate the inhomogeneous version of the cross-type L function.		
10	<i>as.psp</i>		Convert Data To Class psp	Tries to coerce any reasonable kind of data object to a line segment pattern (an object of class "psp") for use by the spatstat package.		
11	<i>distfun</i>		Distance Map as a Function	Compute the distance function of an object, and return it as a function.		
12	<i>mppm</i>		Fit Point Process Model to Several Point Patterns	Fits a Gibbs point process model to several point patterns simultaneously.		
13	<i>anova.mppm</i>		ANOVA for Fitted Point Process Models	Performs analysis of deviance for one or more point process models fitted to replicated point pattern data.		

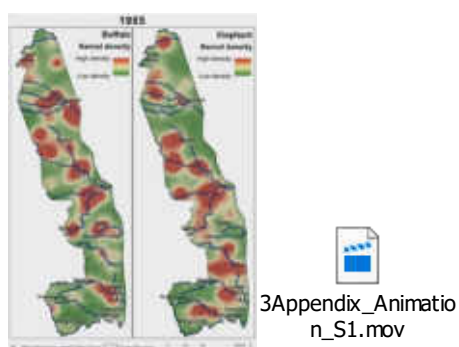
		for Replicated Patterns		
14	<i>Kres</i>	Residual K Function	Given a point process model fitted to a point pattern dataset, this function computes the residual K function, which serves as a diagnostic for goodness-of-fit of the model.	
15	<i>relrisk</i>	Estimate of Spatially-Varying Relative Risk	Generic command to estimate the spatially-varying probability of each type of point, or the ratios of such probabilities.	
16	<i>density</i>	Kernel Smoothed Intensity of Point Pattern	Compute a kernel smoothed intensity function from a point pattern.	
17	<i>stack</i>	Create a RasterStack object	A RasterStack is a collection of RasterLayer objects with the same spatial extent and resolution. A RasterStack can be created from RasterLayer objects, or from raster files, or both. It can also be created from a SpatialPixelsDataFrame or a SpatialGridDataFrame object.	
18	<i>projectRaster</i>	Project a Raster object	Project the values of a Raster* object to a new Raster* object with another projection (coordinate reference system, (CRS)). You can do this by providing the new projection as a single argument in which case the function sets the extent and resolution of the new object. To have more control over the transformation, and, for example, to assure that the new object lines up with other datasets, you can provide a Raster* object with the properties that the input data should be projected to.	<i>raster</i> Hijmans RJ (2016). raster: Geographic Data Analysis and Modeling. R package version 2.5-8. <a href="https://CRAN.R-project.org/package=raster">https://CRAN.R-project.org/package=raster</a>
19	<i>crop</i>	Crop	crop returns a geographic subset of an object as specified by an Extent object (or object from which an extent object can be extracted/created). If x is a Raster* object, the Extent is aligned to x. Areas included in y but outside the extent of x are ignored (see extend if you want a larger area).	
20	<i>overlay</i>	Overlay Raster objects	Create a new Raster* object, based on two or more Raster* objects. (You can also use a single object, but perhaps calc is what you are looking for in that case).	
21	<i>setZ</i>	Get or set z-values	Initial functions for a somewhat more formal approach to get or set z values (e.g. time) associated with layers of Raster* objects. In development.	

22	<i>asImRaster</i>	Convert a raster to an im object	Conversion between rasters and spatstat's im objects	<i>geostatsp</i>	Brown PE (2015). Model-Based Geostatistics the Easy Way. Journal of Statistical Software, 63(12), 1-24. URL <a href="http://www.jstatsoft.org/v63/i12/">http://www.jstatsoft.org/v63/i12/</a> .
23	<i>readShapeSpatial</i>	Read shape files into Spatial*DataFrame objects	The readShapeSpatial reads data from a shapefile into a Spatial*DataFrame object. The writeSpatialShape function writes data from a Spatial*DataFrame object to a shapefile. Note DBF file restrictions in write.dbf.	<i>maptools</i>	Bivand R and Lewin-Koh N (2016). maptools: Tools for Reading and Handling Spatial Objects. R package version 0.8-39. <a href="https://CRAN.R-project.org/package=maptools">https://CRAN.R-project.org/package=maptools</a>
24	<i>bfastmonitor</i>	Near Real-Time Disturbance Detection Based on BFAST-Type Models	Monitoring disturbances in time series models (with trend/season/regressor terms) at the end of time series (i.e., in near real-time). Based on a model for stable historical behaviour abnormal changes within newly acquired data can be detected. Different models are available for modeling the stable historical behavior. A season-trend model (with harmonic seasonal pattern) is used as a default in the regression modelling.	<i>bfast</i>	Verbesselt J, Zeileis A, Herold M (2011). Near Real-Time Disturbance Detection in Terrestrial Ecosystems Using Satellite Image Time Series: Drought Detection in Somalia. Working Paper 2011-18. Working Papers in Economics and Statistics, Research Platform Empirical and Experimental Economics, Universitaet Innsbruck. URL <a href="http://EconPapers.RePEc.org/RePEc:inn:wpaper:2011-18">http://EconPapers.RePEc.org/RePEc:inn:wpaper:2011-18</a>
25	<i>bfmSpatial</i>	Function to run bfastmonitor on any kind of raster brick, with parallel support	Implements bfastmonitor function, from the bfast package on any kind of rasterBrick object. Time information is provided as an extra object and the time series can be regular or irregular.	<i>bfastSpatial</i>	Dutrieux L, DeVries B and Verbesselt J (2014). bfastSpatial: Utilities to monitor for change on satellite image time-series. R package version 0.6.2.
26	<i>chisq.test</i>	Function to run a chi-squared test	Performs a chi-squared contingency table tests and goodness-of-fit test.	<i>stats</i>	R Core Team (2016) R: A language and environment for statistical computing. R Foundation for Statistical Computing, Vienna, Austria. Available from <a href="http://www.R-project.org/">http://www.R-project.org/</a> (accessed October 2013).

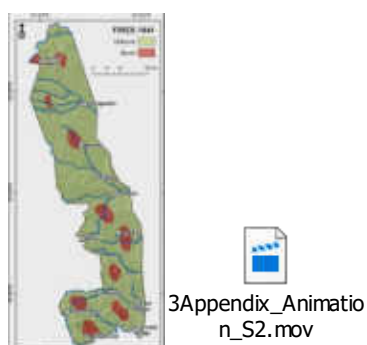
# S5

## Landscape heterogeneity at the interface of herbivore, fire, climate and landform interactions

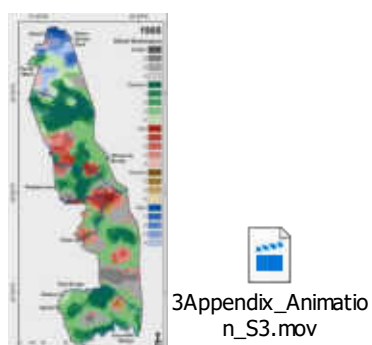
---



**Animation S5.1:** Animation of kernel density estimates of elephants and buffalo from 1985 until 2012.



**Animation S5.2:** Animation of burn scars in the Kruger National Park from 1941 until 2014.



**Animation S5.3:** Animation of spatiotemporal variability of driver dominance over heterogeneity change in Kruger from 1985-2012.

## SUPPLEMENTAL REFERENCES

---

- Baddeley A, Rubak E and Turner R (2015) *Spatial Point Patterns: Methodology and Applications with R*. CRC Press. Taylor & Francis Group, Boca Raton, Florida, USA. ISBN: 9781482210200 - CAT# K21641
- Bivand R and Yu D (2015). *spgwr: Geographically Weighted Regression*. R package version 0.6-28. <https://CRAN.R-project.org/package=spgwr>
- Bivand R and Lewin-Koh N (2016). *maptools: Tools for Reading and Handling Spatial Objects*. R package version 0.8-39. <https://CRAN.R-project.org/package=maptools>
- Brown PE (2015). Model-Based Geostatistics the Easy Way. *Journal of Statistical Software*, 63(12), 1–24. URL <http://www.jstatsoft.org/v63/i12/>
- Brynard HJ (2006) Managing geoscience information in an African context. *PositionIT* March/April: 13–16. Available from <http://www.geoscience.org.za/index.php/publication/downloadable-material> (accessed 16 December 2016)
- Detsch F (2016). *gimms: Download and Process GIMMS NDVI3g Data*. R package version 0.6.0. doi:10.13140/RG.2.1.4824.2962
- Eisenhauer N, Bowker MA, Grace JB and Powell JR (2015) From patterns to causal understanding: Structural equation modelling (SEM) in soil ecology. *Pedobiologia* 58: 65–72. doi:10.1016/j.pedobi.2015.03.002
- Funk C, Peterson P, Landsfeld M, Pedreros D, Verdin I, Shukla S, *et al.* (2015) The climate hazards infrared precipitation with stations - a new environmental record for monitoring extremes. *Scientific Data* 2: 150066. doi:10.1038/sdata.2015.66 2015
- Gollini I, Lu B, Charlton M, *et al.* (2015) *GWmodel: An R Package for Exploring Spatial Heterogeneity Using Geographically Weighted Models*. *Journal of Statistical Software* 63: 1–50

- Govender N, Mutanga O and Ntsala D (2012) Veld fire reporting and mapping techniques in the Kruger National Park, South Africa, from 1941 to 2011. *African Journal of Range and Forage Science* 29: 63–73. doi:10.2989/10220119.2012.697918
- GRASS (2014) GRASS Development Team. GRASS GIS 7.1.svn Reference Manual. Available from <http://grass.osgeo.org/grass71/manuals/index.html> (accessed November 2014)
- Hengl T, Mendes de Jesus J, Heuvelink GBM, Ruiperez Gonzalez M, Kilibarda M, *et al.* (2017) SoilGrids250m: global gridded soil information based on Machine Learning. *PLoS One* 12(2). doi:10.1371/journal.pone.0169748
- Hijmans RJ (2015). raster: Geographic Data Analysis and Modeling. R package version 2.3-40. Available from <http://CRAN.R-project.org/package=raster> (accessed June 2015)
- Hijmans RJ (2016) raster: Geographic Data Analysis and Modeling. R package version 2.5-8. Available from <https://CRAN.R-project.org/package=raster> (accessed 01 December 2017)
- Hijmans RJ, Cameron SE, Parra JL, Jones PG and Jarvis A (2005) Very high resolution interpolated climate surfaces for global land areas. *International Journal of Climatology* 25: 1965–1978. doi:10.1002/joc.1276
- Huang B, Thorne APW, Banzon VF, Boyer T, Chepurin G, Lawrimore JH, Menne MJ, Smith TM, Vose RS, Zhang HM (2017) Extended Reconstructed Sea Surface Temperature, Version 5 (ERSSTv5): Upgrades, Validations, and Intercomparisons. *Journal of Climate* 30: 8179–8205. doi:10.1175/JCLI-D-16-0836.1. Available from [http://origin.cpc.ncep.noaa.gov/products/analysis\\_monitoring/ensostuff/ONI\\_v5.php](http://origin.cpc.ncep.noaa.gov/products/analysis_monitoring/ensostuff/ONI_v5.php) (accessed 20 October 2016)
- Huffman GJ, Adler RF, Bolvin DT, Gu GJ, Nelkin EJ, Bowman KP, *et al.* (2007) The TRMM multi-satellite precipitation analysis (TMPA): quasi-global, multi-year, combined-sensor

- precipitation estimates at fine scales. *Journal of Hydrometeorology* 8: 38–55.  
doi:10.1175/JHM560.1
- Joyce RJ, Janowiak JE, Arkin PA and Xie P (2004) CMORPH: a method that produces global precipitation estimates from passive microwave and infrared data at high spatial and temporal resolution. *Journal of Hydrometeorology* 5: 487–503. doi:10.1175/1525-7541(2004)005<0487:CAMTPG>2.0.CO;2
- Kearney MR, Shamakhy A, Tingley R, Karoly DJ, Hoffmann AA, Briggs PR and Porter WP (2014) Microclimate modelling at macro scales: a test of a general microclimate model integrated with gridded continental-scale soil and weather data. *Methods in Ecology and Evolution* 5: 273–286. doi:10.1111/2041-210X.12148
- Kubota T, Shige S, Hashizume H, Aonashi K, Takahashi N, Seto S, *et al.* (2007) Global precipitation map using satellite borne microwave radiometers by the GSMaP project: production and validation. *IEEE Transactions on Geoscience and Remote Sensing* 45: 2259–2275. doi:10.1109/MICRAD.2006.1677106
- Lefcheck JS (2016) piecewiseSEM: Piecewise structural equation modelling in R for ecology, evolution, and systematics. *Methods in Ecology and Evolution* 7: 573–579. doi:10.1111/2041-210X.12512
- Lefcheck JS and Duffy JE (2015) Multitrophic functional diversity predicts ecosystem functioning in experimental assemblages of estuarine consumers. *Ecology* 96(11): 2973–2983. doi:10.1890/14-1977.1
- Leung Y, Mei C-L, Zhang W-X (2000) Statistical tests for spatial nonstationarity based on the geographically weighted regression model. *Environment and Planning* 32: 9–32
- Leutner B and Horning N (2016) RStoolbox: Tools for Remote Sensing Data Analysis. R package version 0.1.5. Available from <https://CRAN.R-project.org/package=RStoolbox> (accessed 16 December 2016)



- Levick SR and Rogers KH (2011) Context-dependent vegetation dynamics in an African savanna. *Landscape Ecology* 26: 515–528. doi:10.1007/s10980-011-9578-2
- MacFadyen S, Hui C, Verburg PH, Van Teeffelen AJA (2016) Quantifying spatiotemporal drivers of environmental heterogeneity in Kruger National Park, South Africa. *Landscape Ecology* 31: 2013–2029. doi:10.1007/s10980-016-0378-6.
- MacFadyen S, Zambatis N, Verburg PH, Van Teeffelen AJA, Hui C (2018) Long-term rainfall regression surfaces for the Kruger National Park, South Africa: A spatiotemporal review of patterns from 1981-2015. *International Journal of Climatology*. doi:10.1002/joc.5394
- MacFadyen S, Hui C, Verburg PH and Van Teeffelen AJA (*in Review*) Space is not ‘irrelephant’: Spatiotemporal distribution dynamics of elephants in response to density, rainfall, rivers and fire in Kruger National Park, South Africa. *Diversity and Distributions*
- MacFadyen S, Hui C, Van Teeffelen AJA and Verburg PH (*submitted*) Landscape heterogeneity at the interface of herbivore, fire, climate and landform interactions. *Global Change Biology*
- Marshall M, Okuto E, Kang Y, Opiyo E and Ahmed M (2016) Global assessment of Vegetation Index and Phenology Lab (VIP) and Global Inventory Modeling and Mapping Studies (GIMMS) version 3 products. *Biogeosciences* 13: 625–639. doi:10.5194/bg-13-625-2016
- Menne MJ, Durre I, Korzeniewski B, McNeal S, Thomas K, Yin X, *et al.* (2012) Global Historical Climatology Network - Daily (GHCN-Daily), Version 3. NOAA National Climatic Data Center. doi:10.7289/V5D21VHZ (accessed January 2016)
- Muñoz E, Álvarez C, Billib M, Arumí JL and Rivera D (2011) Comparison of gridded and measured rainfall data for basin-scale hydrological studies. *Chilean Journal of Agricultural Research* 71(3): 459–468. doi:10.4067/S0718-58392011000300018

- Naimi B (2015) usdm: Uncertainty analysis for species distribution models. R package version 1.1-12. Available from <http://CRAN.R-project.org/package=usdm> (accessed June 2015)
- NCAR (2014) The climate data guide: precipitation data sets: overview and comparison table. National Center for Atmospheric Research. Available from <https://climatedataguide.ucar.edu/climate-data/precipitation-data-sets-overview-comparison-table> (accessed 25 October 2016)
- Pinzon JE and Tucker CJ (2014) A Non-Stationary 1981-2012 AVHRR NDVI3g Time Series. *Remote Sensing* 6: 6929–6960. doi:10.3390/rs6086929
- R Core Team (2016) R: A language and environment for statistical computing. R Foundation for Statistical Computing, Vienna, Austria. Available from <https://www.R-project.org/>. (accessed 16 December 2016)
- Shipley B (2016) Cause and Correlation in Biology: A User's Guide to Path Analysis, Structural Equations and Causal Inference with R. Cambridge University Press, United Kingdom. ISBN: 0521529212
- Smit IPJ, Smit CF, Govender N, van der Linde M and MacFadyen S (2013) Rainfall, geology and landscape position generate large-scale spatiotemporal fire pattern heterogeneity in an African savanna. *Ecography* 36(4): 447–459. doi:10.1111/j.1600-0587.2012.07555.x
- Sorooshian S, Hsu KL, Gao XG, Gupta HV, Imam B and Braithwaite D (2000) Evaluation of PERSIANN system satellite-based estimates of tropical rainfall. *Bulletin of the American Meteorological Society* 81: 2035–2046. doi:10.1175/1520-0477(2000)081<2035:eopsse>2.3.co;2
- Sun R, Yuan H, Liu X and Jiang X (2016) Evaluation of the latest satellite–gauge precipitation products and their hydrologic applications over the Huaihe River basin. *Journal of Hydrology* 536: 302–319. doi:10.1016/j.jhydrol.2016.02.054

- USGS (2014) Shuttle Radar Topography Mission, 1 Arc-Second Global, Global Land Cover Facility, University of Maryland, College Park, Maryland. Available from <http://dwtkns.com/srtm30m> (accessed 16 December 2016)
- van der Linden P and Mitchell JFB (eds.) (2009) ENSEMBLES: Climate change and its impacts: summary of research and results from the ENSEMBLES project. Met Office Hadley Centre, Exeter, UK. pp. 160
- Vegter JR (1995) Geology map of South Africa with simplified lithostratigraphy for geohydrological use. Water Research Commission TT 74/95
- Venter FJ, Scholes RJ, Eckhardt HC (2003) The Abiotic Template and its Associated Vegetation Pattern. In: du Toit JT, Rogets KH, Biggs HC (Eds.) (2003) The Kruger Experience: Ecology and Management of Savanna Heterogeneity. Island Press, the Center for Resource Economics, Washington, DC, USA. doi:10.2989/10220110409485835
- Vermote E, Justice C, Csiszar I, Eidenshink J, Myneni R, Baret F, Masuoka E, Wolfe R, Claverie M and NOAA CDR Program (2014) NOAA Climate Data Record (CDR) of AVHRR Surface Reflectance, Version 4. [AVH09C1]. NOAA National Climatic Data Center. doi:10.7289/V5TM782M [Accessed December 16, 2016]
- Whyte IJ (2001) Conservation Management of the Kruger National Park Elephant Population. DPhil Thesis. Faculty of the Natural and Agricultural Sciences, University of Pretoria, South Africa
- Wright K (2015) corrgram: Plot a Correlogram. R package version 1.7. Available from <http://CRAN.R-project.org/package=corrgram> (accessed June 2015)